High Rate Reversibility Anode Materials of Lithium Batteries from Vapor-Grown Carbon Nanofibers

V. Subramanian, Hongwei Zhu, and Bingqing Wei*

Department of Electrical and Computer Engineering, and Center for Computation and Technology, Louisiana State University, Baton Rouge, Louisiana 70803

Received: December 5, 2005; In Final Form: February 17, 2006

We demonstrate the high-rate capability of lithium ion insertion−deinsertion reactions in carbon nanofibers (CNFs). The morphology of CNFs with structural and surface defects, due to the mixed features of disordered and graphitic carbon, plays an important role in both the enhancement of the lithium ion storage and the rate-determining reactions during the topotactic process. The reversible specific capacity of the CNFs at a 0.1 C rate was 461 mA·h/g. The most promising property, which is expected to overcome the hurdles of lithium batteries for high-power applications, is that they deliver considerably high specific capacity even at a very high charge−discharge current, i.e., at a cycling rate of 10 C the reversible capacity is around 170 mA·h/g with a 95% Coulombic efficiency.

1. Introduction

Batteries are a critical enabling technology for the development of clean, fuel-efficient vehicles. Among the possible energy storage sources, lithium ion batteries are considered to be one of the most promising power sources for a variety of consumer and military applications. The main advantages of the lithium-based power sources are its lightweight and very high energy density, whereas its disadvantage is lower power density which limits its applicability in various situations especially for electric vehicles (EV). Research for better cathode and anode materials leading to improved electrochemical properties and economical lithium ion batteries is an ongoing pursuit. Most of the commercial lithium ion batteries have $LiCoO_2$ as a cathode material.[1] A variety of other cathode materials, such as $LiMn_2O_4$, $LiFePO_4$, etc., are extensively studied for a possible replacement of the expensive and toxic cobalt oxide cathode which will make lithium ion batteries more cost-effective and environmentally benign.[2]

The development of new high-rate and high-capacity anode materials for lithium ion batteries to match the high-capacity cathodes is of prime importance. There are various anode materials, such as metal oxides, carbonaceous materials, phosphates, and sulfides, etc., that are presently envisaged for use in lithium ion batteries.[3−7] Of all the families of materials studied, carbon-based anode materials always have a range of advantages such as cheap cost, better thermal and chemical stability, eco-friendliness, and ease in preparation in various forms. Of all the carbonaceous materials presently under investigation for use as anode materials for lithium batteries, such as disordered carbons from polymeric or natural precursors, graphite, amorphous carbon, carbon nanotubes, and carbon fibers,[8−12] disordered carbon shows a very high capacity with a very large irreversible capacity, while graphitic carbon shows a lower capacity with a very low irreversible capacity.[7,8] The bamboo-like carbon nanofibers (CNF) demonstrated here exhibit a mixture nature of both the disordered and the graphitic carbon and, therefore, can be expected to perform as a high-rate and high-capacity anode material for lithium ion battery applications.

The topotactic lithium insertion−deinsertion reaction varies with the nature of the host. Typically, metal-oxide-based anode materials mainly show reversible lithium insertion−deinsertion reactions based on the alloying−dealloying of the Li ion and the cation of the metal oxide.[13] In the case of graphitic carbon, it can store up to one Li for every six carbon atoms by a staging mechanism corresponding to a theoretical capacity of 372 mA·h/g.[7] However, the disordered carbon materials can store lithium 2 or 3 times more than the theoretical value for graphite because of the turbostatic disorder of the graphene sheets.[8] Apart from graphitic and disordered carbon materials, other interesting forms of carbon that have evolved after the discovery of fullerenes have also been investigated. Both single-walled and multiwalled carbon nanotubes have been studied for use as negative electrode material in lithium batteries, but no high-rate attempt has been reported.[11]

Studies on carbon fibers as anode materials in lithium batteries have been reported.[12,14−17] However, the carbon fibers so far reported have been much limited to micrometer or submicrometer size in diameter, whereas the total electrochemical response, from the surface film formation to topotactic reaction, will be different when a nanoscopic carbon fiber is used. Different from carbon nanotubes which need a long diffusion time for the lithium ion insertion and deinsertion, the occurrence of defects, including a large number of lattice defects, surface defects along their length, and open ends in CNFs, is expected to show a significant effect on their electronic structure and Li ion battery properties, particularly a shorter diffusion distance for Li ions that is associated with the charge−discharge rate of Li ions. Moreover, to date very little attention has been made on the high-rate capability of this interesting class of materials when used as a negative electrode in a lithium battery. This paper reports the rate capability of CNFs when used as an anode material for lithium batteries. The structural, morphological, and electrochemical properties of CNF materials are discussed, and a model for the lithium insertion−deinsertion and irreversible capacity has been proposed.

* To whom correspondence should be addressed. E-mail: weib@ece.lsu.edu.

10.1021/jp057080j CCC: $33.50
Published on Web 03/16/2006

2. Experimental Section

The CNFs used in this experiment were prepared by a floating catalyst technique.[18] In detail, a quartz tube with an i.d. of 3.5 cm and length of 100 cm is used as a reactor and installed in a horizontal electric furnace. Hexane solutions with a given composition of ferrocene and a small amount of thiophene are introduced into the reactor at a rate of 0.2 mL/min after heating the reactor up to 1150 °C. Typically, for every 100 mL of hexane, 0.5 g of ferrocene and 0.43 mL of thiophene were fed into the chemical vapor deposition (CVD) reactor for the synthesis of CNFs. Hydrogen was used as the buffer gas at a lower rate of 150 mL/min in order to obtain small-diameter CNFs (20 to ~40 nm).[19] The synthesized CNFs showed a narrow pore size distribution of 1 to ~3 nm, and the average surface area determined by the BET N_2 adsorption−desorption method was found to be around 100 m^2/g.[20] The as-grown CNFs were brush collected and were ground in an agate pestle and mortar gently before starting the electrode preparation for the battery.

As-prepared and treated CNFs were characterized by transmission electron microscopy (TEM, JEOL JEM 2010, at an accelerating voltage of 200 kV). The samples were first dispersed in acetone; then after sonication, a drop of this suspension was drop-cast on a carbon-film-coated copper grid. The XRD was done using Cu Kα ($\lambda = 1.54$ Å) radiation and a Siemens D5000 diffractometer in the 2θ range between 10° and 70°.

The electrochemical performance of the CNFs was studied by assembling two-electrode HS-test cells (Hohsen Corp., Japan) with lithium metal as an anode in a 1 M LiPF6 + EC + DEC (1:1 in volume) electrolyte (Ferro Corporation). The electrode materials were prepared by mixing the active material with 10% PVdF/HFP binder (Elf Atofina, France) and 10% conducting carbon black additive in NMP. The well-mixed slurry was coated onto a copper foil using a hand-held doctor blade. The coated foil was allowed to dry in an oven at 110 °C for 1 h and 30 min. Circular disk electrodes were punched from the foil and used as the cathode for assembling the test cells. All manipulations were performed in a glovebox (MBraun, UniLab, U.S.A.) filled with purified argon. The moisture content and oxygen level were less than 5 ppm inside the glovebox. The assembled cells were discharged and charged galvanostatically at different rates from 0.1 to 10 C, between 3.0 and 0.005 V using a potentiostat/galvanostat. Electrochemical impedance spectroscopic (EIS) studies were performed using the same cell setup as described above by applying a small perturbation voltage of 5 mV in the frequency range of 100 kHz to 10 mHz at different voltages during the first discharge−charge cycle. Each impedance measurement was made after an equilibration at the chosen voltage for 1 h. The analysis of the impedance spectra were performed by equivalent circuit software provided by the manufacturer (Autolab FRA/PGSTAT30, EcoChemie, The Netherlands).

3. Results and Discussion

The CNFs were grown in a CVD reactor by a floating catalyst method.[18,19] As shown in Figure 1, the nanofibers consist of stacked curved graphite layers that form "cups". This structure is often referred to as a bamboo type, resembling the compartmentalized structure of a bamboo stem. The chemical and electrical properties of CNFs and carbon nanotubes are expected to be quite different since defect-free nanotube walls do not contain the large amounts of exposed edges and unsaturated bonds of graphene planes, and as a result nanotubes are far less active than nanofibers. Lattice defects and surface defects (Figure 1b) arise mainly in the fiber wall during synthesis. To introduce a substantial number of open-end defects favorable for the diffusion of Li ions into the compartments of the CNFs, the as-prepared CNFs underwent a postgrowth mechanically damaged treatment, resulting in highly defective structures (Figure 1c).

The XRD pattern recorded for the CNFs is shown in Figure 1d. The broad peak profile indicates the disordered nature of the sample with turbostatic ordering. However, the (002) and (101) peaks at $2\theta = 25.5°$ and 45°, corresponding mainly to the graphitized carbon,[18] indicate a mixture feature of the disordered and the graphitic carbon. The lithium insertion reactions in CNF have been studied by using lithium metal as both the reference and counter electrode between 3.0 V and 5 mV.

The electrochemical charge−discharge curves for the first cycle at a 0.1 C rate and that at the 26th cycle for the 10 C rate are shown in Figure 2. The first cycle clearly shows a typical behavior of carbon without any staging mechanism. This indicates that the material is not typical graphitic; if so it would have shown a clear three-stage lithium insertion as reported widely.[21] However, there is a plateau at 0.8 V indicating the surface film formation over the CNF electrode because of the reaction with the electrolyte. This film is ionically conducting and prevents further reaction of the electrode surface with the electrolyte once its thickness reaches such that it can prevent electron tunneling.[7] In the second cycle and beyond there was no such behavior as expected because the film formation reaction is limited to the first cycle. The charge−discharge curves of CNF cycled at a high rate of 10 C is also shown in Figure 2. The lithium ion insertion capacity was 195 mA·h/g, while the deinsertion capacity was 166 mA·h/g, indicating a very high reversible capacity at such high rate of 10 C. To further understand the reactions occurring during the Li insertion, the charge−discharge curves for the first and the 26th cycles were differentiated with respect to the voltage and are shown in the inset of Figure 2, respectively. It can be clearly seen that the film formation reaction is shown in the first-cycle lithium insertion at around 0.8 V. This is absent for any further cycles, indicating that the film formation reaction is a purely irreversible reaction accounting to the first-cycle irreversibility which has a contribution of ~300 mA·h/g, during discharge.

The first-cycle lithium insertion (discharge) capacity was found to be 1261 mA·h/g, and the corresponding reversible capacity was 461 mA·h/g when cycled at 0.1 C. When the cycling rate or the current at which the cell was discharged and charged were increased to 0.75 C there is a little decrease but still at a very high level in the reversible capacity as shown in Figure 3. The CNFs showed excellent cycling behavior even when the current was increased to 2, 5, and 10 C. The remarkable properties of the CNFs allow a very good reversible capacity of about 166 mA·h/g even at a very high current of 3720 mA/g. The reversible capacity stabilized when cycled further at a 10 C rate at 168 mA·h/g after 10 cycles. The Coulombic efficiency increased from 85% for the first cycle at 10 C to 95% for the 10th cycle, which is very promising. This has to be closely observed from the structural and morphological point of view of the CNFs. To the best of our knowledge, this value is extremely high when compared with what has been reported in the literature so far. For instance, the best reversible capacity of ~300 mA·h/g for carbon fiber at the cycling rate of 0.1 C or less has been reported, but it dropped to 100 mA·h/g when the cycling rate was increased to ~3 C.[12,16,17,22,23] The

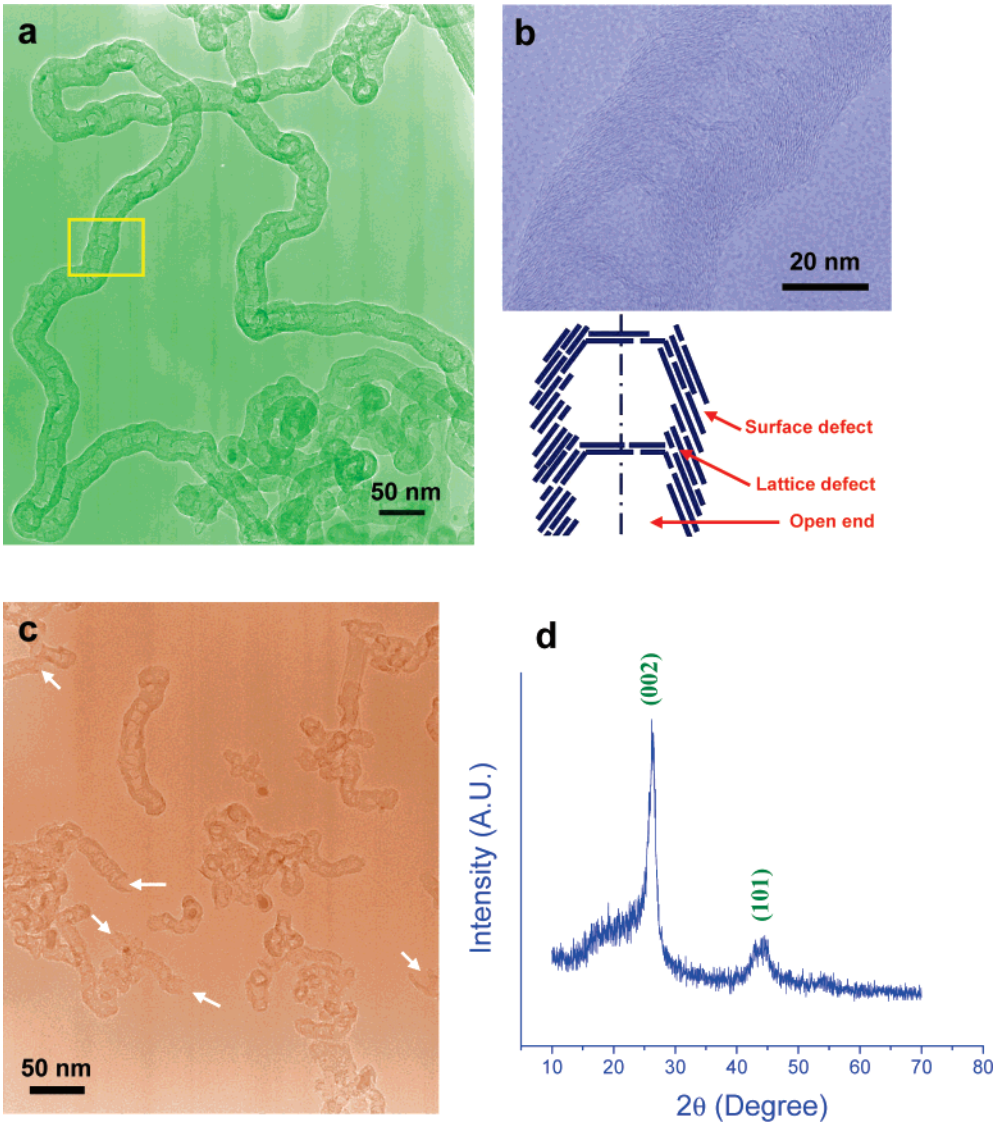

Figure 1. TEM characterization of CNFs. (a) As-prepared CNFs. (b) High-resolution TEM image of a CNF with a simple structural model. (c) Open-end defects introduced by a post-treatment. (d) X-ray diffraction pattern of CNFs.

major difference lies in the structural and dimensional characteristics of the carbon fibers that are reported hitherto and the bamboo type CNFs in the present study.[12,14−17] Various other carbon fibers originating from the pitch-based or polymer-based materials have a dimension close to or greater than 1 μm, as the size of the carbon fiber depends on the method and temperature of preparation.[14−17,22,23] Generally, vapor-grown carbon fibers are expected to show a smaller diameter than those obtained by other methods.[18,19] Another major advantage of the preparation of CNFs by a floating catalyst method here is a continuous production of CNFs, and hence, the scaling for the industrial application is in immediate vicinity and cost-effective when CNFs are envisaged as anode materials in commercial Li ion batteries. However, the main disadvantage of high first-cycle irreversible capacity must be addressed. Further work is in progress to reduce the first-cycle irreversible capacity on this interesting class of CNFs by surface modification processes.

To explain the electrochemical performance of the CNFs, a model based on the structural and morphological arrangement of the CNFs has been proposed schematically in Figure 4. As already shown in Figure 1, the structure of CNFs consists of a lot of stacked curved graphite layers which lead to the formation of a "cuplike" structure in the center as shown in Figure 4a. Apart from their structural arrangement, the CNFs have a large number of lattice and surface defects along their length (open channels due to the stacking arrangement of short graphite layers) and open ends. These lead to a better intercalation and accessibility of the lithium ions to the interior of the CNFs, resulting in both larger irreversible and reversible capacities in the first cycle. As demonstrated in Figure 4b, during Li ion insertion into the CNF (discharge) the ions enter through the open ends of the structure and enter the "cuplike" central part as well. The actual irreversible capacity is much higher than the loss associated with the irreversible film-forming reaction (~300 mA·h/g). This can be attributed to the lithium ions that are inside the cuplike cavity and are irreversibly trapped during the first-cycle insertion (Figure 4c). These trapped lithium ions are not recoverable and amount to a very high irreversible capacity, which in the present case is ~500 mA·h/g. However, the lithium ions inserted into the stacked graphite sheets are very much reversible, and the reversible capacity of the CNFs is much higher than what has been reported for the micrometer-sized carbon fibers. The reason for the increase in capacity is mainly due to the nanoscale size distribution of the fibers, where the smaller fibers have larger surface area and a larger packing fraction than the micrometer-sized fibers. This leads to an

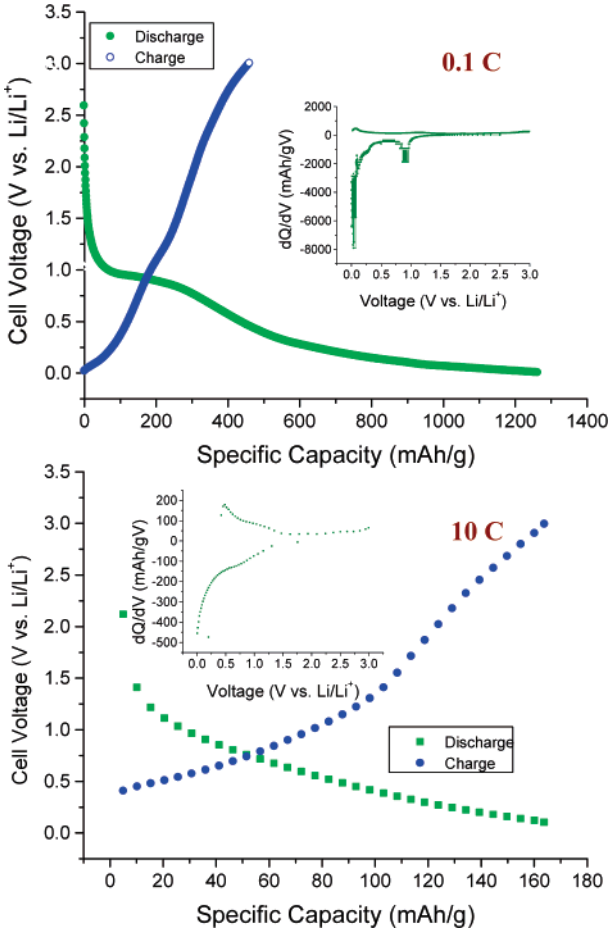

Figure 2. Charge−discharge curves for CNFs at 0.1 and 10 C rates. The insets show the differential capacity plots for the first and the 26th cycle. The cycling was performed in a two-electrode cell with lithium metal as an anode in a 1 M $LiPF_6$/EC/DEC electrolyte. The C rate is defined as follows: a 1 C rate means that if we apply 372 mA/g current for 1 h we can fully discharge the battery, which corresponds to the formation of LiC_6.

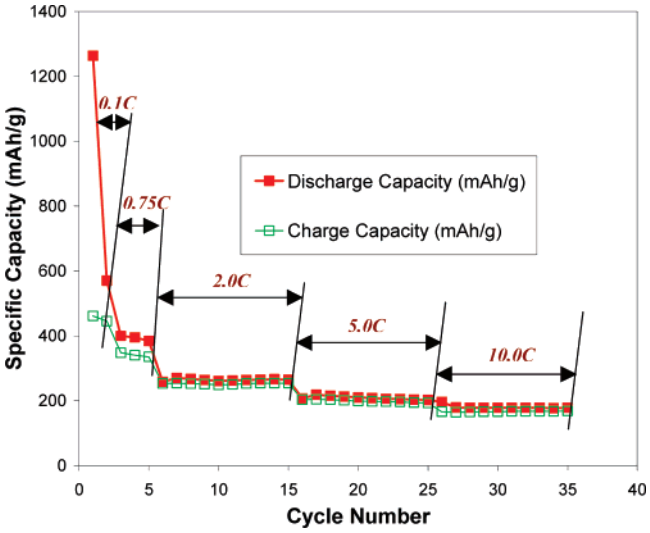

Figure 3. Cycling performance of CNFs at different C rates. The cycling was performed in a two-electrode cell with lithium metal as an anode in a 1 M $LiPF_6$/EC/DEC electrolyte between 3.0 and 0.005 V.

increased uptake of lithium ions up to $Li_{3.3}C_6$ for the insertion and $Li_{1.2}C_6$ for the deinsertion reaction amounting to a loss of 2.1 Li for every 6 carbon atoms.

The most important advantage of the CNFs is their rate capability. As we can see from Figure 3, there has been an excellent reversibility even when the cycling was performed at the rate of 10 C. The structural arrangement of CNFs is so conducive for the lithium ion mobility because of the reduction of the total diffusion length owing to the nanoscale dimensions of the fiber and the stacking arrangement of the short graphitic layers. This is a most favorable factor when the charge−discharge current is high.

The main disadvantage of the conventional electrode material is its diffusion limitation for the Li ion. Overcoming this will enable high-rate performance of batteries. Hence, even when the battery is cycled at more than 3 A/g, the reversible capacity was found to be ∼170 mA·h/g in the present study. In other words, the Li ions that are very much in the curved stacked graphitic sheets respond to a high current well, while those that are closer to the cup-shaped cavity have to overcome a potential barrier to diffuse via the graphitic sheet pathways as shown in Figure 4.

The major advantage of the CNFs reported in the present paper is their suitability to use the same current during both lithium insertion and deinsertion processes. In comparison with the other forms of nanostructured carbonaceous materials, still the electrochemical performance of the CNFs seems to be much better. An excellent rate capability with a specific capacity of 150 mA·h/g was reported when cycled at 2 C for a nanostructured honeycomb carbon anode,[24] but this is much less than what was observed for the CNFs in the present study (reversible capacity of 253 mA·h/g at 2 C).

Many systems respond only to a lower current during the insertion process of Li ions as the surface film or the solid electrolyte interface (SEI) layer formation, surface area, and the lithium diffusion are very critical, especially for graphite.[25−27] Moreover, the structure will be either favorable for the ideal surface film formation or the lithium diffusion.[24] As we have explained earlier, the reason for the first-cycle irreversible capacity is a combination of both surface film formation and the trapping of Li ions in the "cuplike" cavity of the bamboo-shaped CNFs. Also, the diameters of the CNFs are in the range of 20 to ∼30 nm, in which the arrangement of the graphene sheets provides a very favorable environment for the lithium diffusion. Overall, the structural arrangement and proper film formation at the SEI favors a high-rate capability for topotactic reactions for lithium. The aforementioned advantages and the avenue for scaling up of the CNF production to cater to industrial needs make the CNFs a most promising anode material for lithium ion batteries for both low-rate and high-rate applications. To further understand the electrode kinetics of the CNFs during Li insertion, impedance spectroscopic studies were performed.

EIS is an excellent tool to understand the electrode kinetics during lithium ion insertion−deinsertion. The EIS spectra were recorded for the CNFs across Li metal at different voltages during the first lithium insertion−deinsertion cycle, and the typical Nyquist plots consisting of the as-assembled cell impedance and of the cell discharged and charged to 0.6, 0.2, and 0.005 V are shown in Figure 5. As can be seen from Figure 5a for the as-assembled cell, the Nyquist plot only consists of a semicircle in the high-frequency region and a low-frequency spike. As the intercalation level of lithium ion increased, there has been a significant change in the Nyquist plot which shows an additional semicircle in the high- and middle-frequency regions. There is a small semicircle in the high-frequency region attributable to the Li diffusion in the surface film apart from a

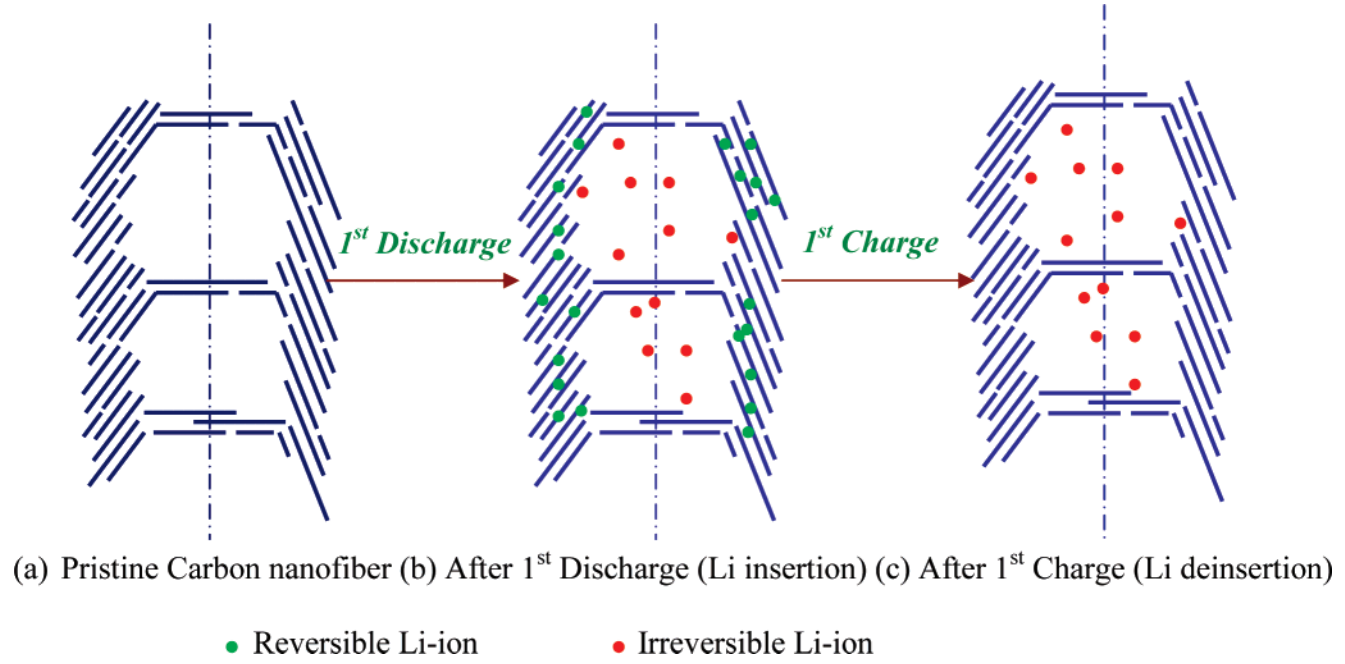

Figure 4. Schematic representation of lithium insertion and deinsertion into the CNF. The irreversible lithium capacity has been reported based on this model.

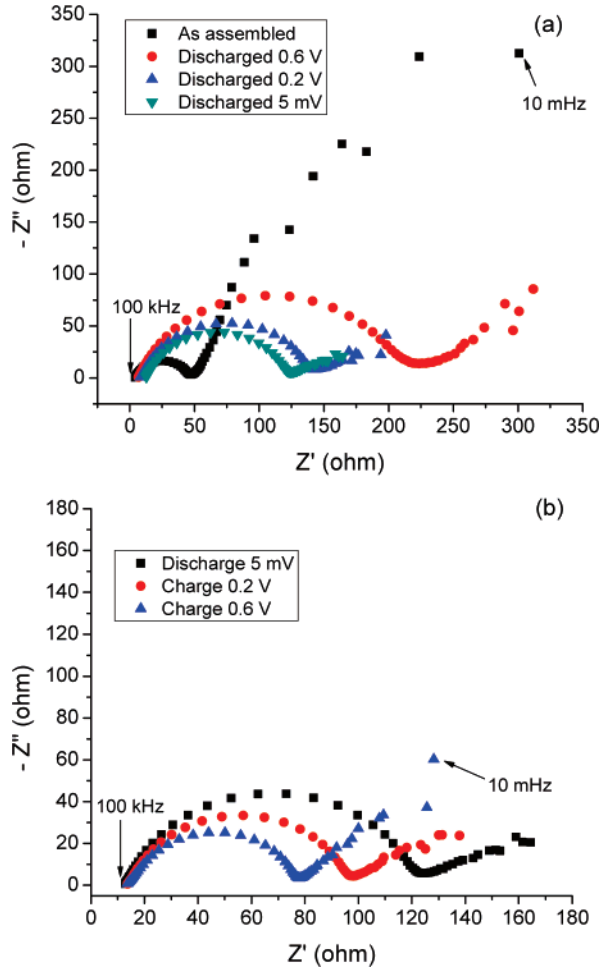

Figure 5. Typical Nyquist plots for CNF during lithium insertion at (a) as-assembled and discharged to 0.6, 0.2, and 0.005 V; (b) discharged to 0.005 V and charged to 0.2 and 0.6 V. EIS was performed at different intercalation voltages in a frequency range of 100 kHz to 10 mHz.

semicircle in the middle-frequency region associated with the charge-transfer reaction. In other words, the charge-transfer resistance is comparatively larger than the resistance of Li diffusion through the surface film, and hence the two semicircles in the high- and middle-frequency are merged and appear to be one. However, the contributions and their associated resistances from the individual processes of Li diffusion in the surface film and the charge transfer across the film electrode interface could be separated by fitting the experimental data using the equivalent circuit model as reported widely.[28−32] In other words, the EIS response of the CNF across metallic lithium can be fragmented as contributions from the diffusion of Li ion in the surface film (high-frequency semicircle), the charge transfer at the surface film electrode interface (middle-frequency semicircle), and finally the diffusion of Li ions in the bulk CNF (low-frequency spike). The diameter of the high-frequency semicircle shows a decrease with respect to the increase in the Li intercalation level. Also, there is a significant decrease in the diameter of the middle-frequency semicircle. Gnanaraj et al.[29] have studied in detail the EIS response of both graphitic and disordered carbon and have found an interesting difference between the two. For both graphitic and disordered carbon, the charge-transfer resistance showed a decrease with respect to the decrease in the intercalation voltage.[29] However, only in the case of disordered carbon a decrease in resistance associated with the surface film is observed when there is a decrease in the intercalation potential. The graphitic carbon showed an increase in resistance associated with the surface film at low potentials.[29,30]

The structural arrangement of the CNFs, however, cannot be categorized either as a pure graphitic or pure disordered one; rather, it is a mixture of both structures. This is well supported by XRD studies as shown in Figure 1, which clearly shows a definite peak profile corresponding to the graphitic carbon with a peak broadening indicating its nanoscale characteristics. Hence, the large first-cycle irreversible capacity arises because of the larger surface area of the CNFs compared to that of the graphitic carbon, while the lithium diffusion process occurs in a similar ordered graphene structure as in a graphitic structure as shown in Figures 1 and 4. In the present case with the CNF electrode, the charge-transfer resistance consistently decreased

with respect to the Li insertion levels until 5mV, similar to what has been observed in the case of both graphitic and disordered carbons.[29,30] The decrease in the diameter of the semicircle in the middle frequency with respect to the increase in the Li intercalation level in the CNF especially for voltages lower than 0.2 V is comparatively lower than that above 0.2 V. This is mainly due to the increase in the Li ion concentration, directly reflecting on the reduction of diffusion of Li ions. This is consistent with the model proposed in Figure 4, where, during the first cycle the Li insertion takes place through the channels and into the central cavity of the bamboo structure of CNFs. As the discharge voltage approaches 0.2 V, the amount of Li ion inserted into the CNFs has increased appreciably with a corresponding charge-transfer reaction leading to a decrease in the diameter of the middle-frequency semicircle. Further decreasing the discharge voltage to 5 mV, the amount of Li ion has almost saturated with the central cavity being filled, leading to a strained Li ion diffusion which hinders the charge-transfer process. This induces only a small decrease in the charge-transfer resistance.

During the first-cycle charging, i.e., the delithiation process, there is again a decrease in the charge-transfer resistance when the cell voltage increases to 0.2 and further to 0.6 V (Figure 5b). This impedance response can be well associated with our model for the first-cycle irreversible capacity. During the Li deinsertion (charging) reaction, there has been a similar decrease in the charge-transfer resistance as Li ions are removed, facilitating a comfortable diffusion of Li ions and hence the charge-transfer reaction as was observed in the case of graphitic structure.[31] This also further supports our model where during the first insertion (discharge) the lithium ions are inserted into the cavity and the side graphene planes, while the removal is mainly limited to that from the side graphene planes as shown in Figure 4.

There have been some earlier studies on a full-cell configuration for Li ion batteries having a micrometer-sized vapor-grown carbon fiber (VGCF) anode and a $LiCoO_2$, $LiNiO_2$, or $LiMn_2O_4$ cathode in a 1 M $LiPF_6$ in EC/DMC electrolyte.[32] The authors have reported an energy density of ~100 W·h/kg for the cell with a VGCF anode and $LiCoO_2$ cathode. The specific capacity of the VGCF reported in their study across Li metal in a half-cell configuration was 328 mA·h/g at a low current of 25 mA/g. With the use of the performance of the CNFs reported in the present study, which showed a specific capacity of 460 mA·h/g at 38 mA/g, the energy density of the full-cell configuration with a well-established $LiCoO_2$ cathode is expected to be exceptionally high. Hence, it is clear that the nanostructure of the CNFs is playing an important role in both higher rate capability and larger reversible capacity, and overcoming or reducing the high first-cycle irreversible capacity will result in a novel anode material for lithium batteries.

4. Conclusions

In conclusion, the vapor-grown CNFs have been demonstrated as a high-rate capable anode material for lithium ion battery. This is the best performance for any carbon fiber reported so far both at low rate and at the very high rate of 10 C. The mechanism of lithium insertion has been proposed, and the reason for the high first irreversible capacity has been attributed to the trapping of the lithium ions in the center of the bamboo-shaped carbon fiber. The high-rate capability for lithium is mainly ascribed to the greater reduction in the diffusion length for the lithium ions and facile structure of CNFs with a lot of structural and surface defects. The promising values with respect to both capacity and rate capability of the half-cell studies for the CNFs clearly indicate their suitability for large-scale applications such as in EVs having the targeted energy density of 75 W·h/kg, and avenues to alleviate the first-cycle irreversible capacity will enable CNFs to reach the commercial stage in near future.

Acknowledgment. The authors gratefully acknowledge financial support from the National Science Foundation under the NSF Award No. DMI-0457555 and the Louisiana Board of Regents under the Award No. LEQSF(2005-08)-RD-B-05.

References and Notes

(1) Nagaura, T.; Tazawa, K. *Prog. Batteries Sol. Cells* **1990**, *9*, 20.
(2) Winter, M.; Besenhard, J. O.; Spahr, M. E.; Novak, P. *Adv. Mater.* **1998**, *10*, 725.
(3) Idota, Y.; Kubota, T.; Matsufuji, A.; Maekawa, Y.; Miyasaka, T. *Science* **1997**, *276*, 1395.
(4) Souza, D. C. S.; Pralong, V.; Jacobson, A. J.; Nazar, L. F. *Science* **2002**, *296*, 2012.
(5) Kim, E.; Son, D.; Kim, T.; Cho, J.; Park, B.; Ryu, K. S.; Chang, S. H. *Angew. Chem., Int. Ed.* **2004**, *43*, 5987.
(6) Yoshio, M.; Wang, H.; Fukuda, K. *Angew. Chem., Int. Ed.* **2003**, *42*, 4203.
(7) Fong, R.; Vonsacken, U.; Dahn, J. R. *J. Electrochem. Soc.* **1990**, *137*, 2009.
(8) Dahn, J. R.; Zheng, T.; Liu, Y. H.; Xue, J. S. *Science* **1995**, *270*, 590.
(9) Fey, G. T. K.; Chen, C. L. *J. Power Sources* **2001**, *97*, 47.
(10) Coutney, I. A.; Dahn, J. R. *J. Electrochem. Soc.* **1997**, *144*, 2943.
(11) Maurin, G.; Henn, F. *Encyclopedia of Nanoscience and Nanotechnology*; American Scientific Publishers: Stevenson Ranch, CA, 2004; Vol. 2, p 773.
(12) Suzuki, K.; Iijima, T.; Wakihara, M. *Electrochim. Acta* **1999**, *44*, 2185.
(13) Coutney, I. A.; Dahn, J. R. *J. Electrochem. Soc.* **1997**, *144*, 2045.
(14) Endo, M.; Kim, Y. A.; Hayashi, T.; Nishimura, K.; Matusita, T.; Miyashita, K.; Dresselhaus, M. S. *Carbon* **2001**, *39*, 1287.
(15) Morita, T.; Takami, N. *Electrochim. Acta* **2004**, *49*, 2591.
(16) Alcantara, R.; Lavela, P.; Ortiz, G. F.; Tirado, J. L.; Stoyanova, R.; Zhecheva, E.; Merino, C. *Carbon* **2004**, *42*, 2153.
(17) Skowronski, J. M.; Knofczynski, K.; Yamada, Y. *Solid State Ionics* **2003**, *157*, 133.
(18) Ci, L. J.; Zhu, H. W.; Wei, B. Q.; Xu, C. L.; Liang, J.; Wu, D. H. *Mater. Lett.* **2000**, *43*, 291.
(19) Ci, L. J.; Li, Y. H.; Wei, B. Q.; Liang, J.; Xu, C. L.; Wu, D. H. *Carbon* **2000**, *38*, 1933.
(20) Ci, L. J. Study on Preparation of Carbon Nanotubes by Floating Catalyst Method and Its Crystallizing Behavior. Ph.D. Thesis, Tsinghua University, Beijing, China, 2000.
(21) Markovsky, B.; Levi, M. D.; Aurbach, D. *Electrochim. Acta* **1998**, *43*, 2287.
(22) Lee, J. K.; An, K. W.; Ju, J. B.; Cho, B. W.; Cho, W.; Park, D.; Yun, K. S. *Carbon* **2001**, *39*, 1299.
(23) Nadeau, G.; Song, X. Y.; Masse, M.; Guerfi, A.; Brisard, G.; Kinoshita, K.; Zaghib, K. *J. Power Sources* **2002**, *108*, 86.
(24) Li, N.; Mitchell, D. T.; Lee, K. P.; Martin, C. R. *J. Electrochem. Soc.* **2003**, *150*, A979.
(25) Buqa, H.; Goers, D.; Holzapfel, M.; Spahr, M. E.; Novak, P. *J. Electrochem. Soc.* **2005**, *152*, A474.
(26) Levi, M. D.; Aurbach, D. *J. Phys. Chem. B* **1997**, *101*, 4641.
(27) Yu, P.; Popov, B. N.; Ritter, J. A.; White, R. E. *J. Electrochem. Soc.* **1999**, *146*, 8.
(28) Choi, Y.-K.; Chung, K.-I.; Kim, W.-S.; Sung, Y.-E. *Microchem. J.* **2001**, *68*, 61.
(29) Gnanaraj, J. S.; Levi, M. D.; Levi, E.; Salitra, G.; Aurbach, D.; Fischer, J. E.; Claye, A. *J. Electrochem. Soc.* **2001**, *148*, A525.
(30) Levi, M. D.; Aurbach, D. *J. Phys. Chem. B* **1997**, *101*, 4641.
(31) Zhang, S.; Ding, S. M.; Xu, K.; Allen, J.; Jow, T. R. *Electrochem. Solid—State Lett.* **2001**, *4*, A206.
(32) Abe, H.; Murai, T.; Zaghib, K. *J. Power Sources* **1999**, *77*, 110.